Supplementary information

Host-guest geometry in paramagnetic cavitands elucidated by ^{19}F electron-nuclear double resonance

Alexey Bogdanov[#, a], Manas Seal[#, a‡], Elad Goren[b], Amnon Bar-Shir[b], Daniella Goldfarb[*a]

[a] *Department of Chemical Physics and Biological Physics, Weizmann Institute of Science, Rehovot 76100, Israel.*

[b] *Department of Molecular Chemistry and Materials Science, Weizmann Institute of Science, Rehovot 76100, Israel.*

[‡] Current address: *Department of Education, Indian Institute of Technology, Kharagpur 721302, WB, India*

Contents

S1. ED-EPR spectra of Gd-α,β-CD compared with those of Gd(III) spin labels

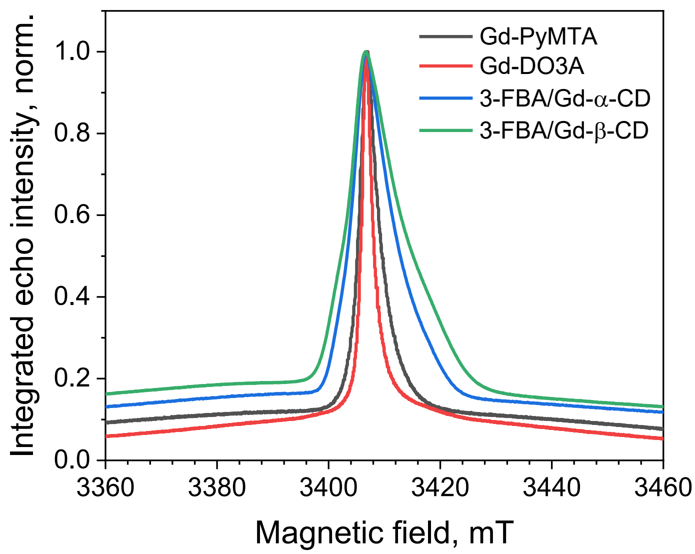

Figure S1. Comparison of the W-band widths of central transitions (CTs) of conventionally used Gd(III) spin labels (Gd-DO3A: BrPSPy-DO3A-Gd(III) complex,[S1] Gd-PyMTA: Gd-F PyMTA ruler[S2]) with 3-FBA/Gd-α-CD and 3-FBA /Gd-β-CD reported in the present work.

S2. Comparison of ^{19}F ENDOR spectra of 3-FBA and 3,5-diFBA guests in Gd-β-CD

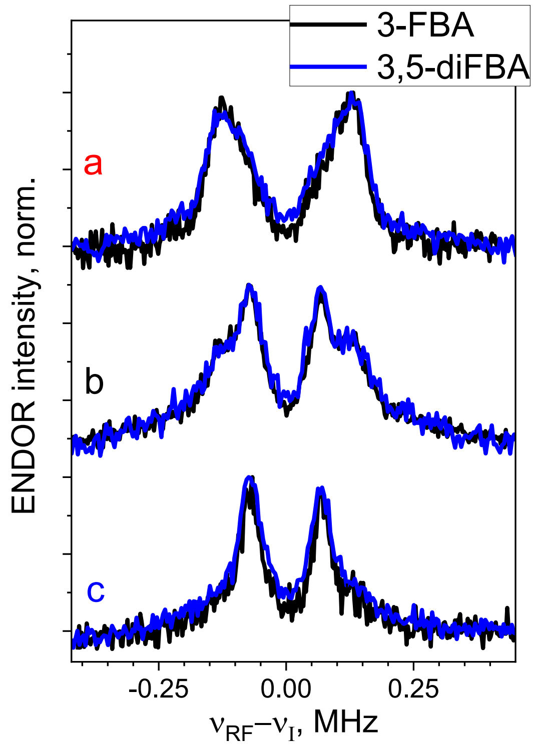

Figure S2. Comparison of the ^{19}F Mims ENDOR spectra of 3-FBA (black lines) and 3,5-diFBA (blue lines) in Gd-β-CD, obtained at magnetic field positions a, b, c, as specified in **Fig. 3B** *(main text)*.

S3. Field dependent ^{19}F ENDOR spectra of different systems and their simulation

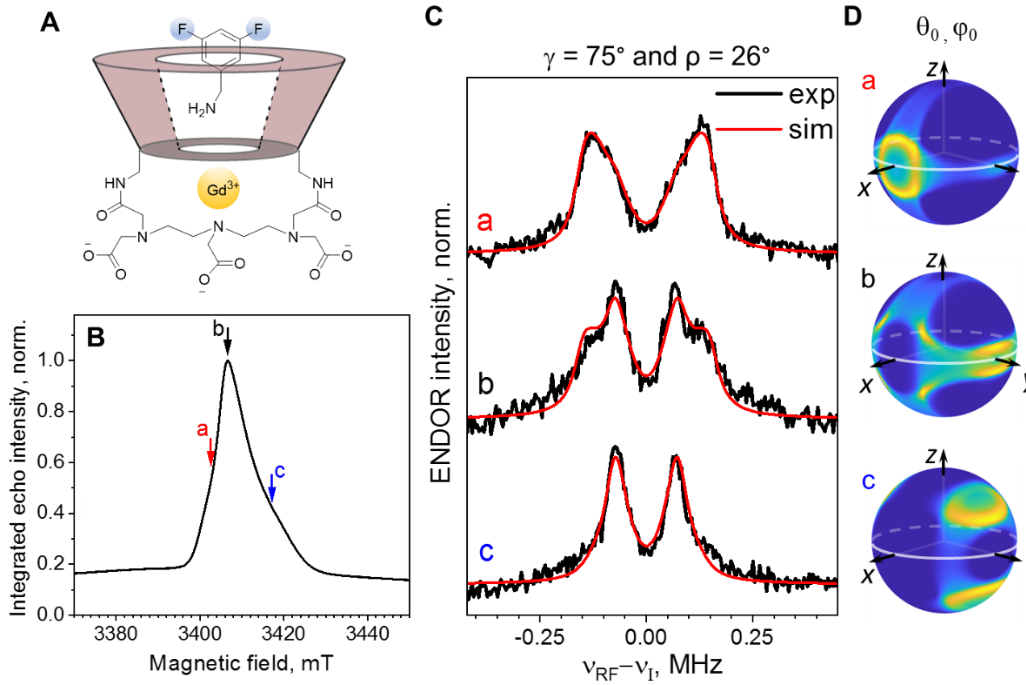

Figure S3. (A) A schematic illustration of 3,5-diFBA/Gd-β-CD. **(B)** The CT region of the ED-EPR spectrum (10K), with the positions at which ENDOR spectra were recorded. **(C)** Experimental ^{19}F ENDOR spectra recorded at –4 mT (a), 0 mT (b) and +11 mT (c) (black) and their simulations (red). **(D)** Heat plots showing the selected orientations θ_0, φ_0 at –4 mT, 0 and 11 mT. The inter-pulse delay τ = 1 μs was used in the Mims sequence.

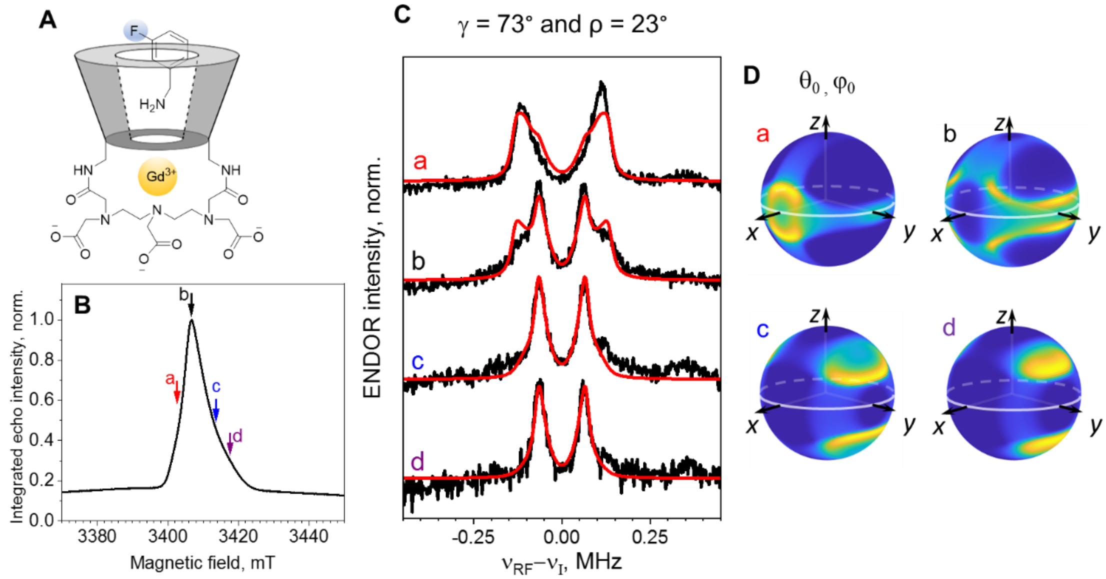

Figure S4. (A) A schematic illustration of 3-FBA/Gd-α-CD. **(B)** The CT region of the ED-EPR spectrum (10K), with the positions at which ENDOR spectra were recorded. **(C)** Experimental ^{19}F ENDOR spectra recorded at –4 mT (a), 0 mT (b), +7 mT (c) and +11 mT (d) (black) and their simulations (red). **(D)** Heat plots showing the selected orientations θ_0 , φ_0 at –4 mT, 0, 7 mT and 11 mT. The inter-pulse delay τ = 1 μs was used in the Mims sequence.

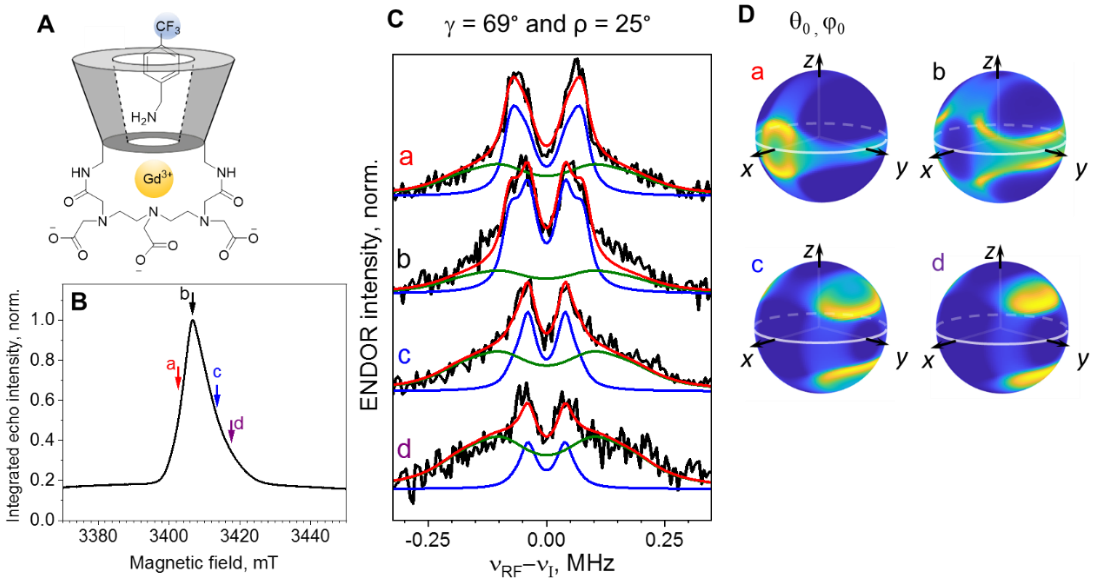

Figure S5. (A) A schematic illustration of 4-CF3BA/Gd-α-CD. **(B)** The CT region of the ED-EPR spectrum (10K), with the positions at which ENDOR spectra were recorded. **(C)** Experimental ^{19}F ENDOR spectra recorded at –4 mT (a), 0 mT (b), +7 mT (c) and +11 mT (d) (black) and their simulations (red). **(D)** Heat plots showing the selected orientations θ_0, φ_0 at –4 mT, 0, +7 and +11 mT. The inter-pulse delay τ = 1 μs was used in the Mims sequence.

S4. Comparison of simulation approaches with/without taking into account orientation selection

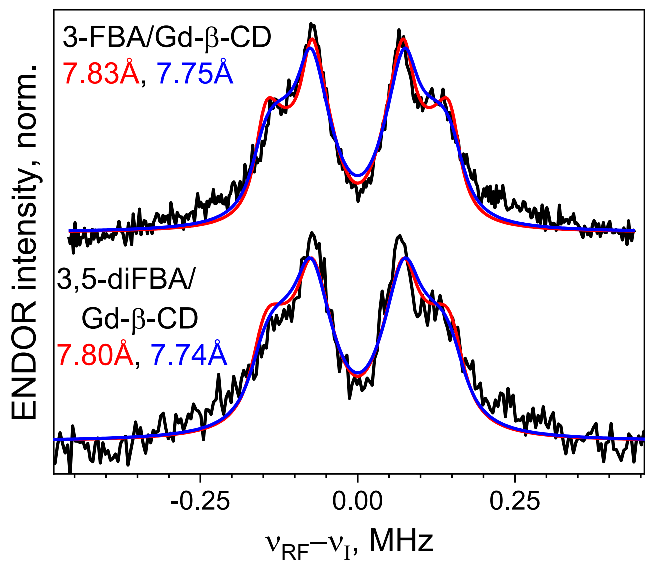

Figure S6. ENDOR spectra of 3-FBA/Gd-β-CD (top) and 3,5-diFBA/Gd-β-CD (bottom) recorded at the field position corresponding to the maximum intensity of EPR spectrum (black lines), best-fit simulations with orientation selection using the orientation distribution from ED-EPR spectral simulation (red lines), best-fit simulation in the absence of orientation selection (blue lines). Gd-F distances obtained using each of the approaches are given in corresponding colors.

S5. Joint simulation of ENDOR spectra of 3,5-diFBA/Gd-α-CD recorded with different τ values

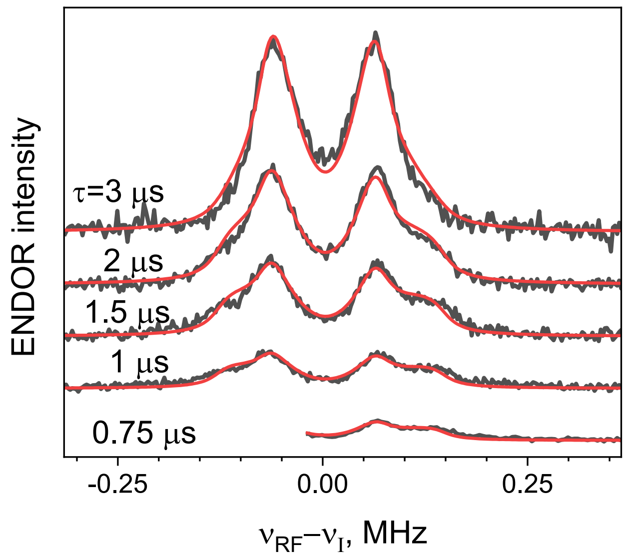

Figure. S7. ENDOR spectra of 3,5-diFBA/Gd-α-CD recorded with different values of the inter-pulse delay τ in the Mims ENDOR sequence (black) and the corresponding simulations (red). The simulation parameters are listed in **Table 2** (*main text*).

S6. ^{19}F ENDOR spectra recorded at the maximum of EPR spectra for all the systems and their simulation

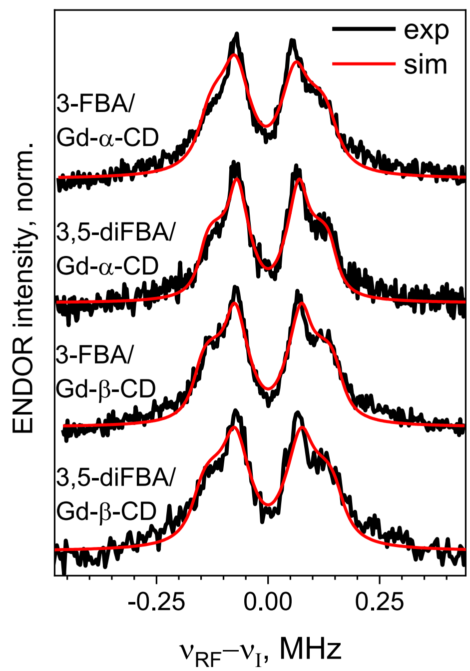

Figure S8. Experimental (black) and simulated (red) ^{19}F ENDOR spectra of 3-FBA,3,5-diFBA/Gd-α,β-CD recorded at the field position corresponding to the maximum of the EPR spectrum of Gd(III). Simulations are done in the assumption of the absence of orientation selection.

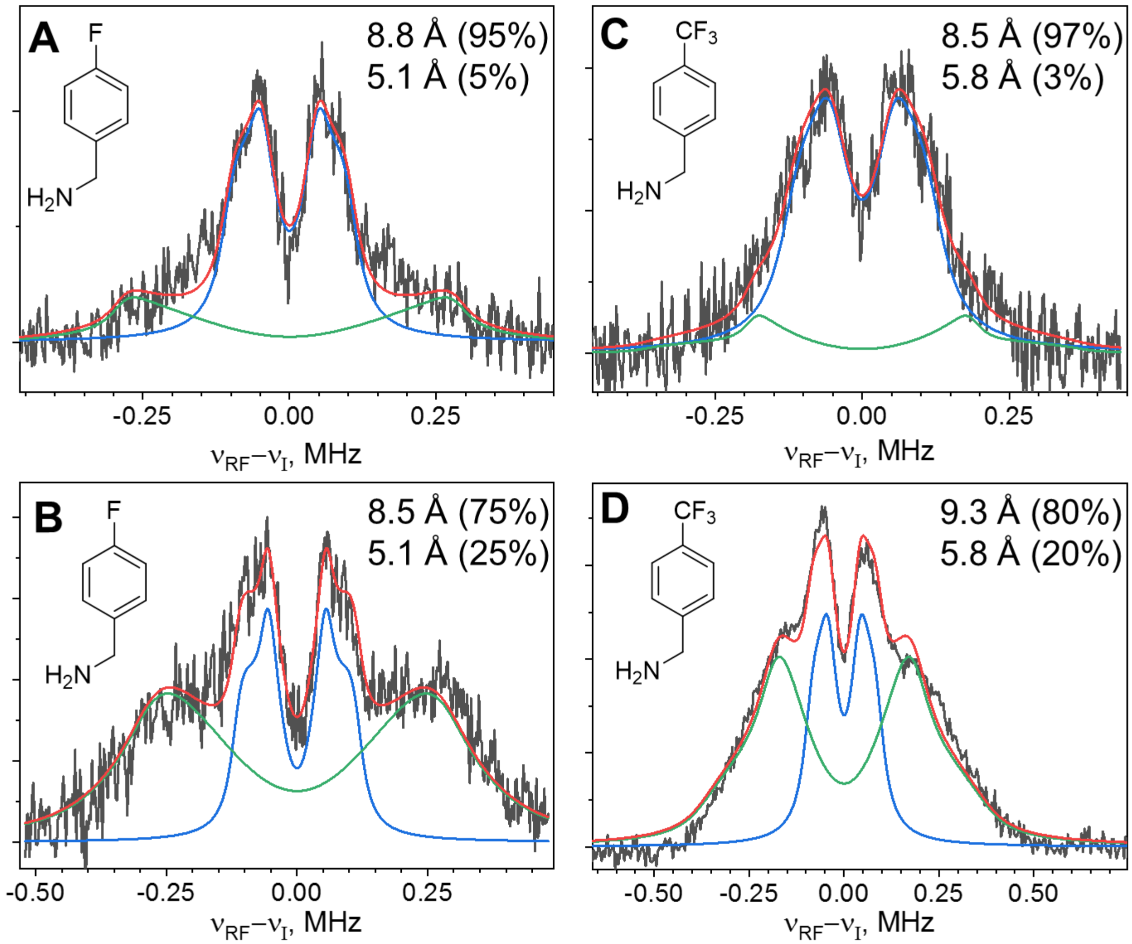

Figure S9. Experimental (black) and simulated (red) ENDOR spectra of 4-FBA **(A,B)** and 4-CF_3BA **(C,D)** in Gd-α-CD (upper panels) and Gd-β-CD (lower panels). The corresponding Gd-F distances and relative populations of the major (blue) and minor (green) contributions are specified in the figure. In these simulations, we assumed identical Gd-F distance for all F atoms in the CF_3. This is a valid assumption for distance larger than 10 Å.[S3] The relatively large integral intensity of the minor populations in panels **(B)** and **(D)** stems from the dramatic increase of ENDOR efficiency with decreasing Gd-F distance r. According to eqs. (2) and (7) of the *main text*, the $\sim 1/r^6$ dependence of ENDOR efficiency holds when $a \cdot \tau \ll 1$. For $\tau = 1$ μs, as used for the presented spectra, this holds up for $a \ll 1$ MHz, thus is applicable in this case.

Supplementary References

S1. Y. Yang, F. Yang, Y.-J. Gong, T. Bahrenberg, A. Feintuch, X.-C. Su and D. Goldfarb, *J. Phys. Chem. Lett.*, 2018, **9**, 6119-6123.

S2. A. Bogdanov, V. Frydman, M. Seal, L. Rapatskiy, A. Schnegg, W. Zhu, M. Iron, A. M. Gronenborn and D. Goldfarb, *J. Am. Chem. Soc.*, 2024, **146**, 6157-6167.

S3. M. Judd, E. H. Abdelkader, M. Qi, J. R. Harmer, T. Huber, A. Godt, A. Savitsky, G. Otting and N. Cox, *Phys. Chem. Chem. Phys.*, 2022, **24**, 25214-25226.